ACADEMIC PRESS

Available online at www.sciencedirect.com

SCIENCE DIRECT®

NeuroImage 18 (2003) 185–197

NeuroImage

www.elsevier.com/locate/ynimg

A multivariate, spatiotemporal analysis of electromagnetic time-frequency data of recognition memory

E. Düzel,[a,*] R. Habib,[b] B. Schott,[a] A. Schoenfeld,[a] N. Lobaugh,[b] A.R. McIntosh,[b] M. Scholz,[a] and H.J. Heinze[a]

[a] *Department of Neurology II, Otto von Guericke University, Leipziger Strasse 44, Magdeburg 39120, Germany*
[b] *Rotman Research Institute, Baycrest Centre, 3560 Bathurst Street, Toronto, Ontario, M6A 2E1 Canada*

Received 1 May 2002; revised 28 August 2002; accepted 21 October 2002

Abstract

Electromagnetic indices of "fast" (above 12 Hz) oscillating brain activity are much more likely to be considerably attenuated by time-averaging across multiple trials than "slow" (below 12 Hz) oscillating brain activity. To the extent that both types of oscillations represent the activity of temporally and topographically separable neural populations, time averaging can cause a loss of brain activity information that is important both conceptually and for multimodal integration with hemodynamic techniques. To address this issue for recognition memory, simultaneous electroencephalography (EEG) and whole-head magnetoencephalography (MEG) recordings of explicit word recognition from 11 healthy subjects were analyzed in two different ways. First, the time course of neural oscillations ranging from theta (4.5 Hz) to gamma (42 Hz) frequencies were identified using single-trial continuous wavelet transforms. Second, traditional analyses of amplitude variations of time-averaged EEG and MEG signals, event-related potentials (ERPs), and fields (ERFs) were performed and submitted to distributed source analyses. To identify data patterns that covaried with the difference between correctly recognized studied (old) words and correctly rejected nonstudied (new) words, a multivariate statistical tool, partial least squares (PLS), was applied to both types of analyses. The results show that ERPs and ERFs are mainly displaying those neural indices of recognition memory that oscillate in the theta (4.5–7.5 Hz), alpha (8–11.5), and to some extent in the beta1 (12–19.5 Hz) frequency range. The sources of the ERPs/ERFs were in good agreement with the topography of theta/alpha/beta 1 oscillations in being confined to the anterior temporal lobe at 400 ms and being distributed across temporal, parietal, and occipital areas between 500 and 700 ms. Gamma oscillations covaried either positively or negatively with theta/alpha/beta1 oscillations. A positive covariance, for instance, was detected over left anterior temporal sensors as early as 200–350 ms and is compatible with studies in rodents showing that gamma and theta oscillations emerge together out of the interaction of the hippocampus and the entorhinal and perirhinal cortices. Fast beta oscillations (20–29.5 Hz), on the other hand, did not strongly covary with slow oscillations and were likely to arise from neural populations not adequately represented in ERPs/ERFs. In summary, by providing a more comprehensive description of electromagnetic signals, time-frequency data are of potential benefit for integrating electrophysiological and hemodynamic indices of brain activity and also for integrating human and animal electrophysiology.

Keywords: Recognition; Oscillations; Wavelets; ERPs; MEG; Source analysis; Partial least squares; PLS; N400; LPC

Introduction

The local synchronized behavior of neural assemblies leads to fluctuations in local field potentials (LFPs) that can be measured using electroencephalography (EEG) and magnetoencephalography (MEG) (Lopes da Silva, 1991). Much of our knowledge about the electrophysiology of recognition memory is derived from the interpretation of EEG and MEG signals that were averaged across multiple trials resulting in the so-called event-related potentials (ERPs) and fields (ERFs). The interpretation of amplitude fluctuations of ERPs and ERFs has provided important insights into the neural mechanisms underlying recognition memory (Dale et

* Corresponding author. Fax: +49-391-67-15233.
E-mail address: emrah.duezel@medizin.uni-magdeburg.de (E. Düzel).

1053-8119/03/$ – see front matter © 2003 Elsevier Science (USA). All rights reserved.
doi:10.1016/S1053-8119(02)00031-9

al., 2000; Duzel et al., 1999; Rugg et al., 1998; Tendolkar et al., 2000). They also continue to be the main source of information for integrating electrophysiological signals and hemodynamic measurements in multimodal imaging. Such multimodal integration is an important goal to achieve in the attempts to understand the functional neuroanatomy of cognitive events.

The utility of ERPs and ERFs for a comprehensive understanding of the electrophysiology of cognitive events and for multimodal integration could be hampered by the limited information they carry about LFP oscillations. Indeed, it has been known for a long time that time-averaged electromagnetic signals provide a limited signature of the electrophysiology of cognitive events. The relationship between ERPs/ERFs and LFP oscillations is determined by the relationship between "evoked" (Galambos et al., 1981) and "induced" (Tallon-Baudry and Bertrand, 1999) neural activity (Basar-Eroglu and Demiralp, 2001). Both types of activity critically differ in how various frequency bands [delta (0.1–3.5 Hz), theta (4–7.5 Hz), alpha (8–11.5 Hz), beta1 (12–19.5 Hz), beta2 (20–29.5 Hz), and gamma (30–80 Hz and higher)] are affected by averaging across trials. Stimulus-evoked neural activity is time- and phase-locked to the onset of a stimulus and, given adequate filtering, is apparent in the averaged EEG and MEG, and hence in ERPs and ERFs. Stimulus-induced neural activity, on the other hand, has a loose temporal relationship to stimulus onset. It consists of oscillatory bursts whose latency jitters from trial to trial. At a given time point after stimulus onset, this type of oscillation will therefore have a different phase on different trials (Tallon-Baudry and Bertrand, 1999). This phase variability will cause attenuation during averaging particularly of beta and gamma oscillations which may therefore become invisible in ERPs and ERFs (Basar-Eroglu and Demiralp, 2001; Varela et al., 2001). Stimulus-induced delta, theta, and alpha frequencies, on the other hand, might also contribute to ERPs and ERFs if their temporal onset does not vary much from trial to trial. Therefore, to the extent that "fast" (above 12 Hz) and "slow" (below 12 Hz) oscillations represent the activity of temporally and topographically separable neural populations, time averaging will cause brain regions with fast oscillations to be underrepresented. Logothetis et al. (2001) recently showed that fast oscillations are very likely to be correlated with the functional magnetic resonance imaging (fMRI) signal. Thus, time averaging of electromagnetic data might lead to discrepancies with hemodynamic measurements to the extent that high-frequency oscillations are not retained in electromagnetic data and do not covary temporally and topographically with slow oscillations that are retained. This problem will be referred to as the problem of high-frequency retention.

The aim of the present study was to investigate the issue of high-frequency retention by characterizing the relationship between ERPs/ERFs and oscillations in the range between 4.5–42 Hz. We identified oscillations during recognition memory and related their time course and topography to the known ERP indices of recognition memory. Comparisons between oscillations and ERFs were performed on the basis of combined ERP/ERF current density source reconstructions rather than ERF field distributions. Amplitudes of oscillations can be more directly compared to current density reconstructions than to field distributions of ERFs, because both types of analyses lack phase information. The technique of wavelet transformation provides a reliable method to measure frequency information of oscillations with high temporal resolution. Tallon-Baudry and Bertrand (1999) have pointed out that in order to identify stimulus-induced oscillations, wavelet transforms must be calculated for single trials of EEG/MEG recordings and the obtained absolute amplitude or the power must be subsequently averaged across trials. Here, we followed this approach and used a combination of EEG and MEG recordings because, due to the relatively low influence of materials with high impedance (e.g., bone) on magnetic compared to electric fields, MEG has a higher topographic specificity than EEG, but much of the existing literature on the electrophysiology of recognition memory is based on EEG recordings. Therefore, the comparison of both data sets allows us to relate MEG findings to existing data.

A major problem in the analysis of oscillations of EEG/MEG recordings is the statistical analysis of the large amount of possible comparisons between electrodes/sensors, conditions, and frequency bands. The traditional approach of performing comparisons between conditions and electrodes/sensors using univariate statistics is somewhat unsatisfactory here because a priori knowledge is required to constrain analysis to a reasonably limited number of statistical comparisons. To achieve a comprehensive analysis of the time-frequency distribution of different oscillations and their topography, and to assess covariance between fast and slow oscillations, we utilized a multivariate statistical analysis tool, partial least squares (PLS) (Lobaugh et al., 2001; McIntosh et al., 1996), that does not require any a priori bias with respect to the location and time course of effects. PLS was not only applied to time-frequency-amplitude information (obtained from wavelet transforms of single-trial MEG data for correctly judged old and new words) but also to ERP/ERF-based spatially normalized (Talairach and Tournoux, 1988) current density reconstructions. By relating the two types of PLS datasets to each other, we were able to determine the frequency bands in which the topography of the amplitude of oscillations was most compatible with the distribution of neural generators identified on the basis of ERPs and ERFs. Additionally, we performed PLS analysis on ERP data alone in order to be able to relate our findings to the preexisting literature on the electrophysiology of memory.

We used a task requiring conscious recognition of studied ("old") and new words. Such recognition is associated with an increase in ERP positivity for the studied words between 400 and 800 ms after the onset of

Table 1
Behavioral results

	Minimum	Maximum	Mean	SD
Hits (%)	51.94	98.61	88.3	14.58
Misses (%)	0.56	6.94	3.3	2.05
Correct rej. (%)	55.00	99.72	89.2	14.05
False alarms (%)	0.28	36.11	5.6	10.25
RT hits (s)	0.57	.96	0.72	0.12
RT misses (s)	0.60	1.20	0.83	0.17
RT correct rej. (s)	0.60	1.01	0.75	0.14
RT false alarms (s)	0.24	1.25	0.86	0.29

Note. RT, reaction times; Correct rej., correct rejections; SD, standard deviation.

word presentation (Duzel et al., 1997; Rugg et al., 1998). This so-called "old/new effect" is composed of an earlier (300 to 500 ms) and more frontal part (henceforth termed N400 effect) as well as a later (500–800 ms) and more parietal part, henceforth called late-positive component, or LPC effect (Curran, 2000; Duzel et al., 1997; Paller et al., 1995; Rugg et al., 1998). Recent data suggest that the inferior temporal cortex is one of the possible generators of the N400 and the LPC effects (Duzel et al., 2001). Using a semantic task (a variant of a living/nonliving judgment) Dale et al. (2000) showed that under indirect task instructions, ERF repetition effects are generated in the inferior temporal and left frontal cortices in the N400 time window. These data cannot be directly related to the explicit recognition task employed here, however, because it has been shown that old/new effects differ in both the N400 and the LPC time window under direct and indirect task instructions (Duzel et al., 2001; Rugg et al., 1998). Therefore, the neural generators underlying the ERP and ERF effects of recognition memory have so far not been sufficiently characterized.

To summarize, the goal of the present study was to investigate the extent to which poor high-frequency retention of ERPs and ERFs causes a loss to brain activity information. To that end, we assessed whether the time course and topography of fast (above 12 Hz) and slow (below 12 Hz) oscillations during recognition memory represent the activity of temporally and topographically separable neural populations. We were thus able to determine if time averaging causes brain regions with fast oscillations to be underrepresented. We hypothesized that the sources of the ERP/ERF old/new effect should be mostly compatible with the topography of amplitude differences between slow oscillations elicited by old and new words. We expected that frequency analyses should additionally identify neural events that oscillate in the beta2 to gamma frequency range but we had no a priori hypothesis as to whether the topography of these fast oscillations would differ from the slower ones and therefore would be less compatible with the location of the sources of ERPs and ERFs.

Materials and methods

Subjects

Fourteen young (age range 20 to 31, mean 24.2), healthy students (10 female) volunteered for paid participation in the experiment. All subjects were right-handed according to self-report and had normal or corrected-to-normal vision. Three subjects were excluded from data analysis due to high levels of scanner/ambient noise and movement artifacts.

Stimulus presentation

The experiment was divided into 30 blocks that consisted of a study and test phase. The stimuli consisted of words (Celex Database (Baayen et al., 1993), mean word frequency 46, 4 to 9 letters per word, text height 2 cm, approximate visual angle 5.2°). During each study phase, 12 words were presented visually on a backprojection screen at a distance of 100 cm. The interstimulus interval (ISI) was 2 s and the stimulus duration was 1.2 s. Subjects were instructed to make a pleasant-unpleasant judgment on each study word, responding with their index finger for words that they felt were pleasant and with their middle finger for words which they felt were unpleasant. Each study phase was followed by a test phase. The test list comprised the 12 studied ("old") words and 12 unstudied ("new") words in a random order. The test words were presented in lists of three (ISI 2 s, stimulus duration 600 ms) with a blink pause between each list. Subjects were instructed to indicate whether they had seen the word during the study phase or not. They were instructed to press the index finger for old words and the middle finger for new words. Subjects were told to carry out all responses with their right hand during the first 15 study-test blocks and with their left hand during the second 15 blocks.

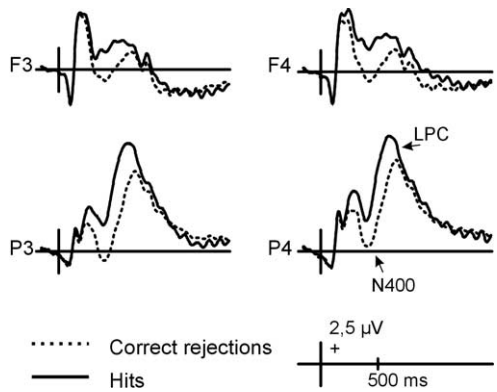

Fig. 1. Grand average (11 subjects) event-related potentials (ERPs) elicited by correctly recognized studied words (hits, solid lines) and correctly rejected unstudied words (dotted lines). F3/F4: left and right frontal electrodes. P3/P4: left and right parietal electrodes. On electrode P4, the three parts of the ERP that display differences between hits and correct rejections are labeled; P275, positive peak at 275 ms; N400, negative peak at 400 ms; LPC, late-positive component peaking at 500–600 ms.

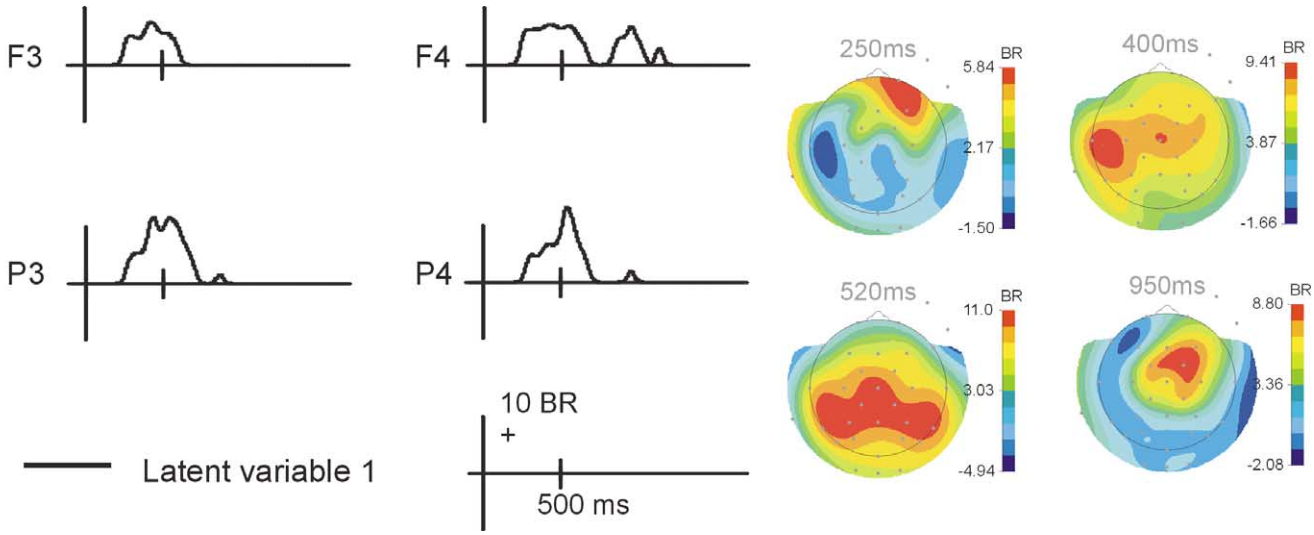

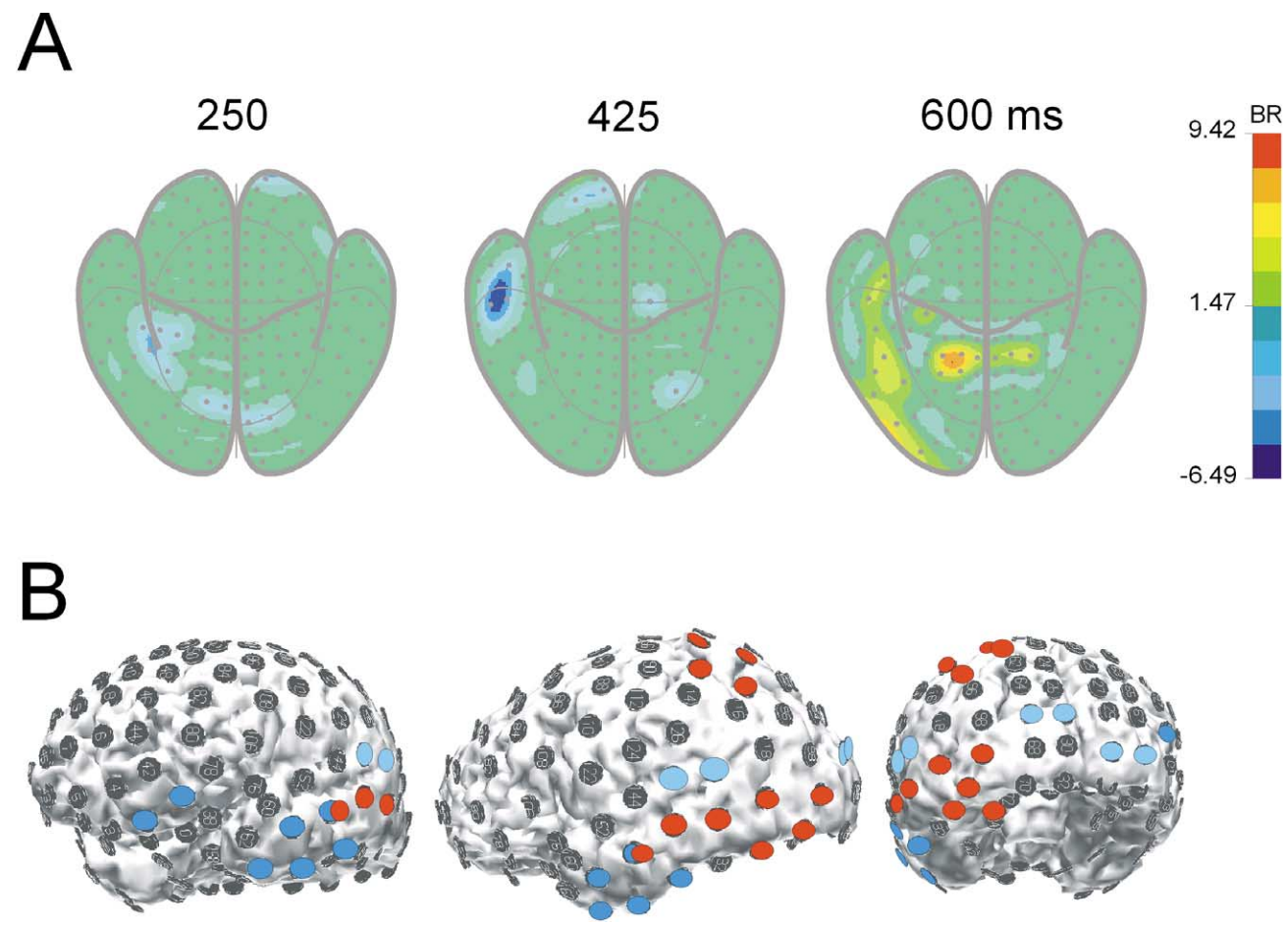

Fig. 2. Results of the first latent variable (LV) from the partial least-squares (PLS) analysis of the averaged ERPs elicited by hits and correct rejections. This LV distinguishes electrodes whose activity differentiates between hits and correct rejections. Both the waveforms (on the left) and the spline interpolated topographic maps (on the right) display the bootstrap ratios of the electrode saliences to their standard errors at each time point (Hits are displayed in reds [positive values], whereas Correct Rejections are displayed in blues [negative values]). Bootstrap ratios above 1.96 are considered to represent reliable effects. Electrode labels in on the left are the same as in Fig. 1.

Fig. 3. Results of the first LV from the partial least-squares (PLS) analysis of current density (CD) reconstructions (linear least-squares minimum norm method; ERPs and ERFs were fitted together) calculated for hits and correct rejections. This LV distinguishes brain locations whose activity differentiates between hits and correct rejections. The spline interpolated topographic maps (A) display the bootstrap ratios of the source-location saliences to their standard errors at each time point (Hits are displayed in reds [positive values], whereas Correct Rejections are displayed in light blue at 250 ms and dark blue at 425 ms [both negative values]). Bootstrap ratios above 1.96 are considered to represent reliable effects. The source locations are 164 regions evenly distributed

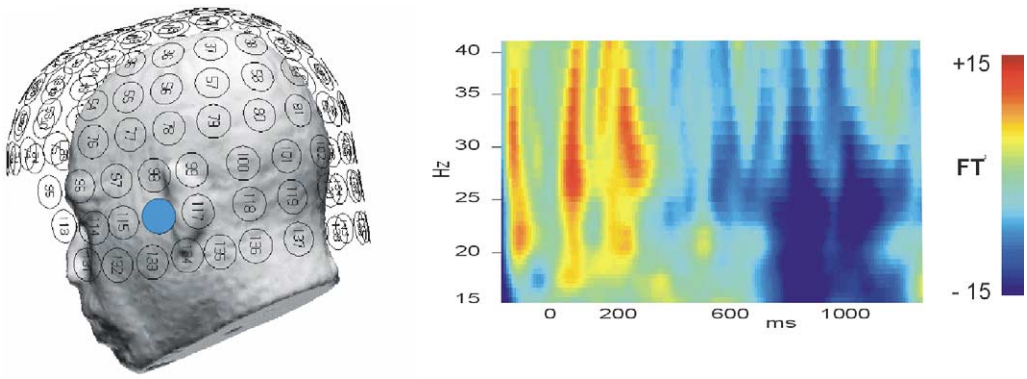

Fig. 4. Time-frequency amplitude spectra for hits obtained by wavelet transformation. The *x* axis denotes the time after stimulus onset in ms. The *y* axis denotes frequency in Hz. Amplitude is coded as color. Time-frequency amplitude was calculated for single artifact-free trials and than averaged across all trials of hits and all 11 subjects. The sensor location is illustrated by a blue circle with respect to a subject's scalp.

Recording and analysis

Electroencephalography and magnetoencephalography signals were registered simultaneously with a digitization rate of 254 Hz and filtered (IIR-Butterworth filter) with a bandpass from DC to 50 Hz. EEG was recorded from 29 electrodes (Fz, Pz, Cz, Oz, Inz, Fp1, Fp2, F3, F4, F7, F8, T3, T4, C3, C4, P3, P4, In1, In2, T5, T6, FC1, FC2, CP1, CP2, PO1, PO2, TO1, TO2) mounted on an electrode cap (Lectron Engineering, Helsinki, Finland) and referenced to the left mastoid. Horizontal eye movements were recorded from an electrode behind the right lateral orbital angle and referenced to an electrode at the left lateral orbital angle. Eye blinks and vertical eye movements were recorded from an electrode below the right orbital limb and referenced to the left mastoid. EEG and EOG signals were amplified using a 32-channel Synamps amplifier (NeuroScan Inc., Hemdon, VA) and coregistered with the MEG signals. MEG signals were recorded using a 148-channel BTi Magnes 2500 whole-head magnetometer (Biomagnetic Technologies Inc., San Diego, CA) and submitted to on-line and off-line noise reduction (Robinson, 1989). Prior to recording, individual skull/scalp landmarks were digitized (left and right preauricular points, Cz, nasion, inion) using a Polhemus 3Space Fastrak system. The positions of all EEG electrodes were also digitized.

EEG and MEG epochs (single-trial raw data) for correctly recognized old words (hits) and correctly rejected new words (correct rejections) underwent separate artifact rejection. Artifact thresholds were 3.5 pT for MEG and 100 μV for EEG. Event-related potentials from the EEG epochs and event-related fields from the MEG epochs were derived by averaging the artifact-free epochs from −200 ms prestimulus to 1800 ms poststimulus. The baseline offset (−200 to 0 ms) was corrected after averaging. The mean number of trials contributing to the average was 180 hits and 190 correct rejections for the ERPs and 220 and 230 correct rejections for the ERFs.

Source analysis

All source analysis (Curry, Version 4, Neuroscan Inc., 2000) was performed using a realistic head model (boundary element model, BEM; Hämäläinen and Starvas, 1989) to account for the different conductivities of brain/CSF, bone, and skin. The BEMs were obtained from a segmented anatomical MRI scan (3D SPGR [spoiled gradient echo]) of each subject. Each BEM consisted of three triangle nets for brain/CSF, bone, and skin. EEG and MEG field distributions were fitted in conjunction with the EEG data referenced to a common average for this purpose. With a common realistic volume conductor, the MEG shows only a weak dependence on the electric properties of the different compartments. This requires that the conductivities of the volume conductor model are matched for the EEG and MEG recordings. A conductivity factor was therefore determined to scale the EEG data with respect to the MEG data on the basis of a tangential dipole evoked by tactile stimulation of the index finger by an air puff at 30 to 40 ms latency (Fuchs et al., 1998). Reliably across these subjects, the conductivity factor could be approximated to 0.8 and this value was used for all subjects. Current densities were computed on individual boundary element models restricted to the cortex surface (the cerebellum was excluded to sim-

in Talairach space. On the maps, the circle marks the vertical level of the AC-PC line ($z = 0$), while the diagonal marks the horizontal level of the AC-PC line ($y = 0$). The time information on each map denotes the time after stimulus onset in ms. (B) A single subject's brain with the 164 regions indicated by circles (they correspond in location to the "flattened" Talairach space in part A) is displayed from a left antero-lateral view (left), from a left side view (middle), and from a left postero-lateral view (right). The colored regions illustrate the locations of the regions in part B. Blue circles correspond to areas with relatively higher CD values for correct rejections (light blue at 250 ms and dark blue at 425 ms) while red regions correspond to areas with relatively higher CD values for hits.

plify the model, but might have contributed to the recorded electromagnetic activity) using the linear least-square minimum norm method (User Guide Curry, Version 4, 2000 (Fuchs et al., 1999; Hopf et al., 2001)). Signal-to-noise ratios (SNRs; high SNRs are critical for a good source reconstruction) of EEG and MEG data were estimated within a time window of 0 to 700 ms with respect to a 200-ms baseline preceding each stimulus onset (by "noise" we mean neural activity in the baseline period that is allegedly uncorrelated with the old/new status of the stimulus). Current density distributions were computed every 4 ms for the time windows from 250 to 630 ms. To ensure the best possible SNRs, this analysis was performed separately for hits and correct rejections rather than for the difference waveforms between them. After source analysis, the individual cortex models with the current density distributions of the 11 subjects were spatially normalized into the Talairach and Tournoux reference frame (Talairach and Tournoux, 1988). The current density distributions were then partitioned into 164 regions of similar size that evenly covered the entire brain volume. This was achieved by summing up the current strengths of elementary dipoles in cortical regions with an average diameter of 2 cm (Fig. 6B). The current densities thus obtained for these 164 regions were submitted to PLS.

To summarize, we have attempted to improve the accuracy of source localization by using realistic head models (Crouzeix et al., 1999), combining EEG and MEG data (Fuchs et al., 1998), having a high number of trials and a good SNR (Fuchs et al., 1999). Also, to maximize SNR, we have based our source analyses on unsubtracted waveforms for hits and correct rejections (which also has the advantage of avoiding artifacts due to nonlinearities in brain activity). However, the inferior temporal cortex and medial temporal region are, due to their distance to the recording sensors and electrodes, prone to estimation errors of current density reconstructions in the order of 1–2 cm (Crouzeix et al., 1999; Fuchs et al., 1998).

Frequency analysis

After artifact rejection, a continuous wavelet transformation was applied to single trials of MEG in each sensor, using Morlet wavelets at 0.5 Hz intervals in the 4.5 to 42 Hz range. A Morlet wavelet is a complex function of time (t) and frequency (f) with the shape of a gaussian filtered sinusoid as defined in

$$w(t,a) = \mathrm{sqrt}(1/a)*e(j*wo*t/a) \cdot *e^{(-(t/a)_{2/2})}, \qquad (1)$$

where wo is the central frequency of the wavelet (2π); a is a scaling factor selected to cover a frequency range from 4.5 to 42 Hz; t is the time domain vector at each scaling factor, and j denotes complex notation.

For each frequency (i.e., scaling factor) the wavelet was convolved with the MEG signal. The resulting time-frequency coefficient matrix was averaged across all epochs separately for hits and correct rejections. The modulus of the resulting average complex coefficients denoted the absolute amplitude (square root of the power) for each frequency at each time point (the codes for the wavelet transformation were written in Matlab and are available from the author upon request). The amplitude values were z-normalized for each subject to account for the fact that slower frequencies have higher amplitude values than faster frequencies. The mean amplitude of designated frequency bands was then calculated and used for topographical illustration and PLS analysis. These frequency bands were theta (4.5–7.5 Hz), alpha (8–9.5 and 10–11.5 Hz), beta 1 (12–19.5 Hz), beta 2 (20–24.5 and 25–29.5 Hz), and gamma (30–42 Hz).

Partial least-squares analysis

Statistical analysis on ERPs, MEG, and EEG source, and MEG frequency data was performed by the multivariate partial least-squares method (Lobaugh et al., 2001). PLS is a statistical technique similar in nature to principal components and factor analyses that examines the relationship between a set of exogenous measures such as orthogonal contrast vectors coding for the experimental design and measures of brain activity (ERPs, CSDs, time-frequency data). The PLS procedure consists of three steps. (1) The computation of a correlation matrix between orthogonal contrast vectors coding for the experimental design (one vector per degree of freedom [df]) and measures of brain activity (electrode/sensors $\times$ time) across both subjects and tasks. This cross-correlation procedure produces one correlation map (consisting of electrode/sensors $\times$ time number of columns) per contrast vector. (2) The correlation maps generated in step 1 are combined into a matrix and decomposed with singular value decomposition (SVD). SVD produces a df number of mutually orthogonal variables (latent variables, LVs), each consisting of a singular image (electrode/sensor salience) and a singular profile (design salience). The singular image identifies sensors/electrodes at particular points in time whose activity covaries, as a whole, with different components of the experimental design. The singular profile identifies the components of the experimental design that most strongly are related to the pattern revealed in the singular image. (3) Multiplication of the singular image by the raw electrode/sensor spatiotemporal data (dot product) for each subject results in individual scalp scores. The scalp score is an indication of how much of the pattern represented in a singular image is expressed by a subject within a condition and is conceptually similar to a factor score in factor analysis. For a detailed description of PLS see McIntosh et al. (1996); for a description of the application of PLS to EEG, see Lobaugh et al. (2001). To determine the stability of the saliences identified on the LVs, the standard errors of the saliences were estimated through bootstrap resampling (Braun et al., 1998; Efron and Tibshirani, 1986; Fabiani et al., 1998). Bootstrap samples

were generated using sampling with replacement, keeping the assignment of experimental conditions fixed for all subjects. PLS was recalculated for each bootstrap sample. No corrections for multiple comparisons were necessary because the saliences were calculated as a whole. A salience whose value depends greatly on which subjects are in the sample is less precise than one that remains stable regardless of the sample chosen (Sampson et al., 1989). The ratio of the salience to the bootstrap standard error is approximately equivalent to a *z*-score if the normality of the bootstrap distribution is valid (Efron and Tibshirani, 1986). Data points where the salience was greater than twice the standard error ($P < 0.05$) are considered reliable. To test the statistical significance of each latent variable, each subjects' data were randomly reassigned without replacement to different experimental conditions, and the entire PLS procedure was repeated. Following 500 such randomizations, the number of times the singular value from the randomized PLS analysis exceeded the singular value from the original PLS analysis was noted, thus providing an exact probability.

Results

Behavioral results

Table 1 summarizes the proportions and reaction times for hits, correct rejections, misses (new responses to old words), and false alarms (old response to new words) as well as the corresponding reaction times (RTs). RTs to hits were 30 ms faster than RTs to correct rejections (one-factorial ANOVA, $F(1, 10) = 21.7$, $P = .001$).

Event-related potentials

Event-related potentials to hits and correct rejections started to differ at 250 ms after the onset of word presentation (Fig. 1). LV1 from the PLS analysis distinguished hits from correct rejections beginning at 250 ms (Fig. 2) over right frontal electrodes. At 400 ms, this effect shifted toward left fronto-central recording sites. Later the topography shifted toward bilateral temporal and parietal areas, being more prominent over the left. A right frontal effect distinguished hits and correct rejections between 900 and 1500 ms.

Current density reconstructions

Mean SNRs in the first 700 ms after stimulus onset were 12.2 (SD 4.2) for hits and 13.8 (SD 5.2) for correct rejections in the MEG data and 22.3 (SD 11.5) for hits and 20.4 (SD 9.2) for correct rejections in the EEG data. LV1 from the PLS analysis distinguished the current densities (at the 164 source locations in Talairach space) for hits and correct rejections beginning at 250 ms (Fig. 3). Between 250 and 450 ms, correct rejections were associated with higher current densities than hits. Until 350 ms, this difference was most prominent over the left superior temporal gyrus, Brodman area (BA) 22, left cuneus (BA 18), and right middle occipital gyrus, lingual gyrus, and posterior portions of the fusiform gyrus (BA 18). At 400 ms, it shifted toward the anterior portions of the left middle temporal gyrus (BA 21 and 38), inferior temporal gyrus and fusiform gyrus (BA 20), and left middle frontal gyrus (BA 11) (Fig. 3). From 450 ms until 630 ms, hits were associated with higher current densities than correct rejections in the left inferior occipital gyrus (BA 19), middle occipital gyrus (BA 18), fusiform gyrus (BA 37), middle temporal gyrus (BA 21), and left parietal neocortex including superior and inferior parietal lobule (BAs 7 and 19), cuneus (BA 40), and angular gyrus (BA 39). No significant effects were observed after 630 ms.

Frequency analyses

Averaged wavelet transforms of artifact-corrected MEG single epoch data revealed clear time-frequency-amplitude distributions for each sensor (Fig. 4). Maps of these time-frequency-amplitude distributions showed topographical differences between hits and correct rejections across various frequency bands. Furthermore, while for theta, alpha, and beta1 frequencies the amplitude was higher at occipito-parieto-temporal sensors after stimulus onset than in the baseline period before stimulus onset (red regions in Fig. 5), the amplitude in the beta2 and gamma range also showed a decrease (blue regions in Fig. 5). Slower frequencies (theta and alpha) contributed most strongly to the frequency amplitude over fronto-temporal sensors in the time window of the LPC, while, in the earlier time windows, all frequency ranges could be measured, with the faster frequencies being more posterior than the slower ones.

PLS of the time-frequency data for hits and correct rejections yielded three significant LVs, all of which dissociated the two classes of stimuli. Fig. 6 illustrates the corresponding time-frequency-sensor patterns in topographic maps that display the bootstrap ratios of the sensor saliences to their standard errors at each time point for each LV. Red colors denote time windows and areas which show a positive correlation with the corresponding LV pattern, whereas blue colors denote time windows and areas in which such correlations are negative. All frequency bands contributed to all three LVs. The first LV discriminated hits from correct rejections mainly in the beta2 frequency band maximally at 400 ms and over left fronto-parieto-temporal sensors. Here, hits were associated with higher beta2 amplitudes than correct rejections. The second LV discriminated hits from correct rejections in the theta, alpha, and beta1 frequency bands with the gamma band showing the reverse pattern. Hits were associated with higher theta, alpha, and lower beta amplitudes than correct rejections over parieto-temporal, bilateral parieto-occipital, and right frontal sensors prior to 350 ms. At 425 ms, this difference was confined to the left anterior

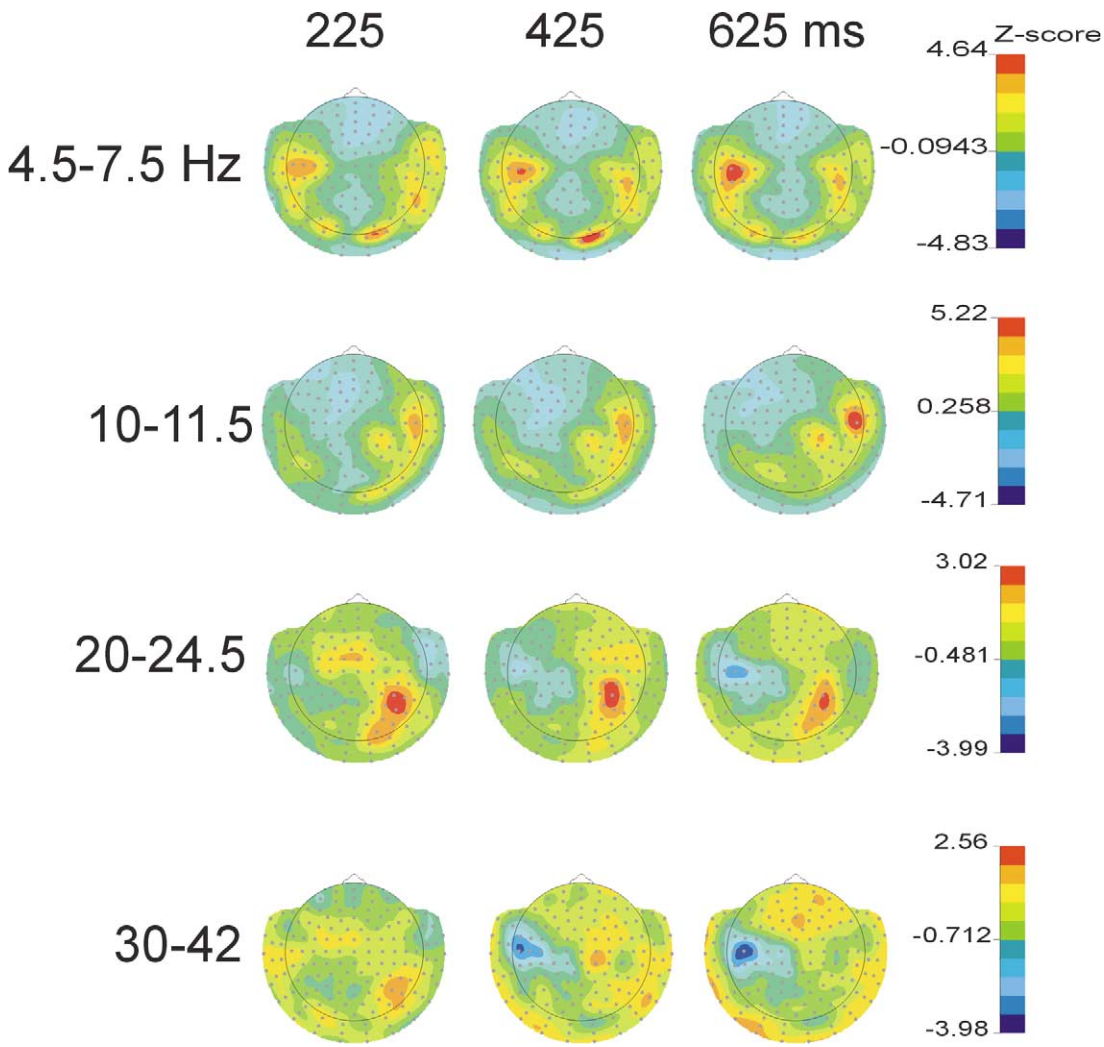

Fig. 5. Topographic maps of the mean z-normalized time-frequency amplitude across designated frequency bands collapsed over hits and correct rejections. Positive z-scores indicate an increase of amplitude and negative z-scores a decrease in amplitude with respect to a baseline of 200 ms preceding the stimulus onset. For each depicted time window, the mean z-score across 100 ms is plotted.

temporal sensors, while between 500 and 850 ms it was distributed over three distinct peaks over fronto-temporal, fronto-parietal, and occipital areas. In all three time windows, correct rejections were associated with higher gamma amplitudes than hits over these sensor sites. The third LV showed that the theta, alpha, and gamma frequency bands similarly discriminated between hits and correct rejections, being opposite to the beta band. Between 200 and 350 ms hits were associated with higher theta, alpha, and gamma amplitudes over left anterior temporal sensors.

In all three LVs, very late (after 1000 ms) differences were found between hits and correct rejections (Fig. 7). As can be seen in Fig. 7, the amplitude patterns reversed in this late time window. In LV1, correct rejections were associated with higher beta2 amplitudes than hits over bilateral parieto-occipital sensors; in LV2, they were associated with higher theta, alpha, and beta1 amplitudes over right parietal and left frontal sensors; and in LV3, they were associated with higher theta and alpha amplitudes over right fronto-temporal, left parietal, and left posterior and inferior temporal sensors.

Discussion

Partial least squares identified fast (gamma and beta) and slow (alpha and theta) oscillations that distinguished hits (old) from correct rejections (new) at different time points after stimulus onset and different sensor locations (Fig. 6). PLS of time-averaged ERP/ERF source models (Fig. 3) showed that old/new differences were compatible mainly with the time course and topography of slow oscillations including beta1, but not beta2, frequency bands. Unlike beta2 oscillations, gamma oscillations did covary (positively and negatively) with slow oscillations, which indicates that they, albeit not visible in ERPs/ERFs, were generated by similar neural populations that also generated slow oscillations (Fig. 6). Additionally, PLS of time-fre-

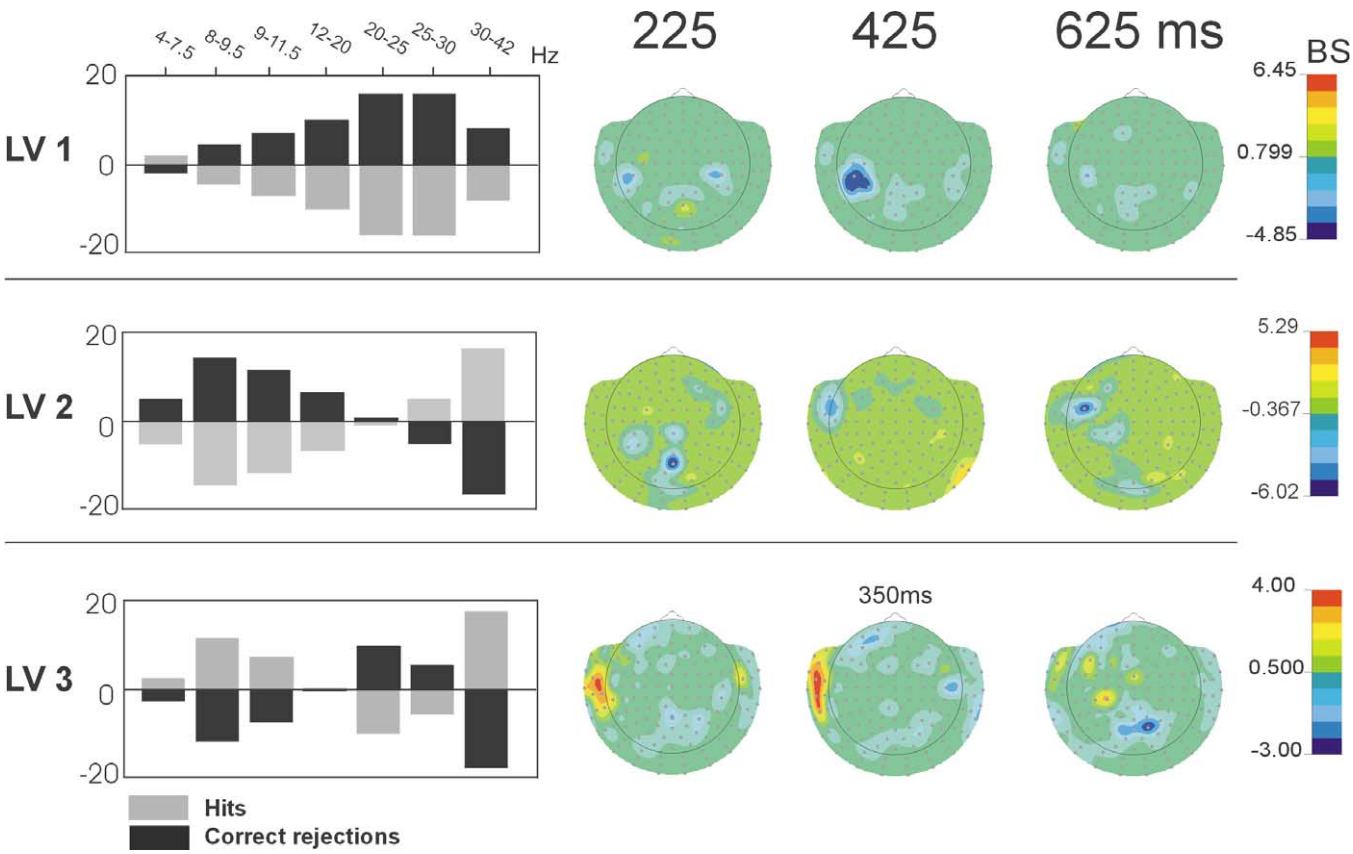

Fig. 6. Results of the three significant LVs from the partial least-squares (PLS) analysis of the time-frequency data for hits and correct rejections illustrates which time-frequency-sensor patterns dissociate hits from correct rejections. Plotted on the left are the frequency scores for each frequency band in the "Hits" (gray) and "Correct Rejections" (black) conditions. On the right, spline interpolated topographic maps display the bootstrap ratios of the sensor saliences to their standard errors at three time points for each LV. Bootstrap ratios above 1.96 are considered to represent reliable effects. In the topographic maps, red colors denote time windows and areas which correlate positively with the corresponding LV pattern, whereas blue colors denote time windows and areas in which such correlations are negative. The top figure shows the results from LV1. This LV mainly discriminates hits from correct rejections in the beta2 but not alpha and theta frequency bands. The middle figure shows the results from LV2. This LV mainly discriminates hits from correct rejections in the theta, alpha, beta1, and gamma frequency bands. The bottom figure shows the results from LV3. This LV demonstrates that the theta, lower alpha, and gamma frequency bands similarly discriminate between hits and correct rejections.

quency data revealed old/new differences in late time windows (after 1000 ms) and in locations, where ERPs and ERFs did not show reliable effects (Fig. 7). Hence, our results indicate that time-frequency analyses identify fast oscillating brain activity that is not adequately represented in time-averaged ERP/ERF signals.

Current density reconstructions

PLS revealed that different current density distributions dissociated old and new words in the early (250 to 350 ms), the N400 (350 to 450), and the LPC (450 to 630 ms) time windows (Fig. 3) all of which preceded the subject's old/new motor response. The findings support the inference made from topographic analyses of ERPs in previous studies that the old/new effects in these time windows are mediated by different neural structures (Curran, 2000; Rugg et al., 1998) rather than just reflecting quantitative amplitude differences. Between 250 and 350 ms, the neural sources of the old/new effect were located over left superior temporal gyrus (BA 22), left cuneus (BA 18), right middle occipital gyrus, lingual gyrus, and posterior portions of the fusiform gyrus (BA 18). This bilateral extrastriate and lateral temporal location of the early old/new effect changed in the N400 time window, such that between 350 and 450 ms it shifted anteriorly and inferiorly and was confined to a left anterior inferior temporal generator. Invasive ERP recordings in patients with intractable epilepsy has also shown old/new effects in explicit word recognition paradigms (as used here) in the anterior portion of the inferior temporal lobe, in the N400 time window (so-called AMTL-N400) (Elger et al., 1997; Fernandez et al., 1999; Grunwald et al., 1998; Heit et al., 1990; Smith, 1987). In the LPC time window, source differences between repeated and new words were distributed over posterior regions of the left parietal lobe, occipital, and posterior inferior temporal cortices, unlike in studies of implicit memory experi-

ments where they were mainly confined to left frontal regions (Dale et al., 2000).

Time-frequency-amplitude distributions

Oscillations in the various frequency bands showed increases as well as decreases in amplitude when compared to their baseline values (Fig. 5). Such event-related synchronization (ERS), e.g., an increase in amplitude, and event-related desynchronization (ERDS), e.g., a decrease in amplitude, have been observed in many cognitive studies (Burgess and Gruzelier, 2000; Pfurtscheller and Aranibar, 1977). However, our PLS analysis was designed to identify time-frequency-amplitude-sensor patterns that dissociated old and new words from each other, independent of whether that dissociation was accompanied by an ERS or ERDS for both types of stimuli. As can be seen in the three LVs in Fig. 6, PLS showed that old and new words did differ in the amplitudes of slow as well as fast oscillations. In the first LV the difference was mainly in the beta2 frequency range, in the second LV it was in the theta/alpha/beta1 and gamma ranges (Fig. 6) and in the third LV, it was in the theta/alpha and gamma ranges. Thus, of the fast oscillations, only gamma covaried temporally and topographically with slower oscillations (negatively in LV2 and positively in LV3) while beta2 oscillations did not. The poor high-frequency retention in ERPs/ERFs can therefore be expected to be associated with a loss of information about the activity of brain regions that participated in recognition memory in the beta2 frequency range. Indeed, as will be discussed in turn, some evidence for this can be seen in the fact that brain regions identified by source analyses of ERP/ERF data were not compatible with the topography of the beta2 oscillations.

Comparisons between source and frequency analyses

A direct comparison of the results obtained by the source analysis of ERP/ERF data and the frequency data would require the identification of the sources of oscillations. In the present experiment these sources were not known and comparisons were therefore inferential. Also, because we used single-epoch raw data for the frequency analyses, the sensor locations of the oscillations identified here were associated with an intersubject variability of approximately 2 cm due to differences in relative head positions between subjects. Nevertheless, comparisons of the source locations for ERP/ERF differences between old and new words and the topography amplitude differences in the three LVs show that mainly slow (theta/alpha) oscillations and to some extent beta1 oscillations as identified in LV2 are likely to be represented in the ERPs/ERFs. This correspondence holds for all three time windows in which the current density analyses revealed distinct patterns, 250 to 350, 350 to 450, and 450 to 630 ms. Most strikingly, the theta, alpha, and beta1 oscillations were confined to left anterior temporal sensors in the N400 time window (Fig. 3), where, at the same time, the source analysis identified a left anterior temporal source for the old/new ERP/ERF effect (Fig. 6). In the LPC time window, these oscillations were distributed over fronto-temporal, fronto-parietal, and occipital sensors, where, at the same time, the source analysis identified distributed generators over temporal, parietal, and occipital sensors. The ERP field distributions (Fig. 2) with a right frontal old/new effect at 250 ms, a left fronto-temporal old/new effect around 400 ms, and a mostly left parietal old/new effect in the LPC time window were also in agreement with the topography of theta/alpha/beta1 oscillations observed in LV2.

One major discrepancy between ERP/ERF-based results and the topography of oscillations concerned left frontal old/new differences in LV1 and LV2. Unlike the ERP/ERF-based results, the oscillations identified in LV1 and LV2 appeared to have a prominent left frontal contribution (Fig. 6). Left frontal old/new effects are in good agreement with fMRI results that have also shown left prefrontal recognition effects (Henson et al., 1999). Our results suggest that the reason why left prefrontal recognition effects do not become apparent with ERP/ERF-based analyses to the same extent as with frequency analyses is due to the poor high-frequency retention in ERPs and ERFs. These prefrontal effects oscillate in the beta2 frequency range in LV1 and in the alpha/beta1 frequency range in LV2. Albeit to a lesser extent than beta2 oscillations, alpha and beta1 oscillations can already be expected to be attenuated by time-averaging across trials.

Another discrepancy between the results of the source and the frequency analysis was apparent in the time window between 250 and 450 ms. While old words were associated with higher amplitude values of theta, alpha, and beta frequencies in this time window, the source strengths were higher for new words. This discrepancy could point toward differences in phase variability for old and new words in this time window; there might be a higher variability in phase for old than for new words. A higher variability in phase would not affect the amplitude of oscillations derived from single-trial analyses. However, it would diminish the amplitude of the time-averaged ERPs due to cancellation effects across trials. Whether such differences in phase variability exist for hits and correct rejections remains to be determined in future studies.

Potential implications for multimodal imaging

Logothetis et al. (2001) have recently investigated which electrophysiological index of neuronal activity most closely correlated with the hemodynamic BOLD signal. Using simultaneous acquisition of fMRI and intracortical recordings, they demonstrated that LFPs correlate much more closely with the BOLD signal than single- and multiunit activity. LFPs that correlated with the BOLD signal showed a broad frequency range from delta to gamma, but the

higher correlations were observed with the faster frequencies. While it is not yet clear to what extent these frequency characteristics of the correlations between LFPs and the BOLD response are specific to the paradigm Logothetis et al. used (visual checker board stimulation) and to the brain regions from which they recorded (primary visual cortex), these findings demonstrate that the averaged broadband ERP and ERF responses often utilized to combine electromagnetic data and fMRI data will only display a limited aspect of the data and that correlations between the two techniques are likely to be better if high-frequency information is also considered. This is of considerable importance when one attempts to relate fMRI and MEG data. FMRI, has for instance shown left prefrontal recognition effects (Henson et al., 1999). Our PLS of the frequency-amplitude data show that such repetition effects may emerge in the beta2 frequency range early (LV1) or alpha and beta1 frequency range later on (LV2) but not appreciably contribute to the ERP/ERF-based source solutions.

A related problem becomes apparent in the results of all three LVs. In a very late time window (after 1000 ms), after subjects had made recognition memory judgments (Fig. 7), old/new effects emerged that were different in topography and magnitude from the effects observed prior to the subjects' old/new decision. These very late effects might be related to the encoding of new stimuli rather than being part of earlier retrieval processes. This possibility is supported by the observation that new words were generally associated with higher amplitude oscillations than hits in this time window. To the extent that these very late old/new effects are associated with fast stimulus-induced oscillations they will not appear in time-averaged ERP/ERF signals and hence will not be visible in any source analysis based on such signals. Such very late fast oscillations will, however, contribute to old/new differences measured with fMRI and might therefore cause additional discrepancies between fMRI results and ERP/ERF data.

Links to animal physiology and lesion data

Animal studies and in vitro investigations indicate that alpha and beta oscillations might play a crucial role in the transfer of information from MTL structures to neocortical areas as well as in the representation of distributed neocortical information. Beta oscillations are able to synchronize neural populations over long conduction delays (Kopell et al., 2000) and might be suitable for the functional coupling of remotely distributed brain regions. A similar interpretation might be true for alpha frequencies, which, rather than being variations of the physiological alpha rhythms observed during resting, might reflect the modulation of brain structures specific for memory functions, such as the hippocampus and connected neocortical areas (Buzsaki, 2002; Schurmann and Basar, 2001; Niedermeyer, 1997; Pfurtscheller and Aranibar, 1977). At the cortical level, generators of the alpha rhythm are likely to be the distal parts of the dendrites of pyramidal cells (Steriade et al., 1990). Based on the observation that hippocampal output via the subicular and entorhinal cortex backprojects to these distal parts of cortical dendrites, Burgess and Gruzelier (2000) have proposed that alpha oscillations and their modulations might reflect memory-related cortical operations modulated by the hippocampal system. Thus, during retrieval, the alpha and beta oscillations observed in LV2 might be important for a hippocampally dependent large-scale integration of information across brain areas distributed over temporal, fronto-parietal, and occipital regions, a mechanism suitable for the retrieval of episodic information that is rich in contextual detail and is critically dependent on the integrity of the hippocampal formation (Rolls, 1996; Vargha-Khadem et al., 1997). Indeed, theta/alpha/beta1 oscillations dissociated old and new words over distributed brain regions between 250 and 350 ms (parieto-temporal, bilateral parieto-occipital, and right frontal sensors) and in the time window of the LPC (fronto-temporal, fronto-parietal, and occipital sensors). Of these two time windows, only ERP effects in the latter, the LPC time window, have so far been linked to episodic memory and it has been shown that they are abolished by relatively isolated hippocampal injury (Duzel et al., 1997, 2001; Paller et al., 1995; Rugg et al., 1998; Klimesch et al., 2000, 2001). Whether the distributed oscillations of LVs between 250 and 350 ms are dependent on hippocampal intergrity remains to be established. There is some indication that this might be the case. Duezel et al. reported that in a patient with bilateral hippocampal injury ERP old/new effects in this early time window differed from normals (Duzel et al., 2001).

In LV3, theta/alpha and gamma oscillations covaried in an early time window until approximately 350 ms after stimulus onset. Investigations in the rodent brain have shown that theta (Green and Arduini, 1954; Vanderwolf, 1969) and gamma (Basar et al., 2001) are prominent rhythms within the septohippocampal system and the entorhinal cortex (O'Keefe and Burgess, 1999; Petsche et al., 1962). It has been proposed that theta and gamma are likely to interact in the transfer of information between the hippocampus and the neocortex (Buzsaki, 1996) and that gamma and theta oscillations are coupled such that gamma bursts occur within designated periods of the theta phase. Hippocampal theta oscillations are not limited to rodents (Buzsaki, 2002) and could also be demonstrated in humans using MEG recordings (Tesche and Karhu, 2000). It is thus possible that the covariance of theta/alpha-gamma oscillations observed over left anterior temporal sensors in LV3 is generated in the hippocampal formation together with the entorhinal cortex. It should be noted here that the rodent theta rhythm overlaps with the human alpha rhythm (Buzsaki, 2002).

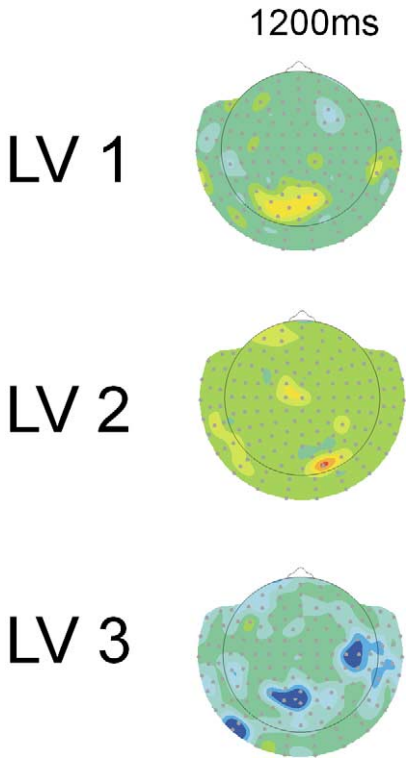

Fig. 7. Results of the first three LVs in three very late time windows. The LV patters are as depicted in Fig. 6. The scales and LV contrasts are the same as in Fig. 6.

Summary

Our results show that poor high-frequency retention of ERPs/ERFs leads to a loss of brain activity information due to a lack of covariance between fast and slow oscillations. In multimodal imaging, this is likely to cause discrepancies between electromagnetic and fMRI data because fast (beta2) oscillations can be expected to make considerable contributions to the BOLD signal. Our data indicate that during recognition memory such discrepancies might be found for left prefrontal activity. Unlike beta2, gamma oscillations did covary with slow oscillations. This suggests that gamma oscillations, at least for the type of recognition memory tested here, will not cause appreciable discrepancies between ERPs/ERFs and hemodynamic measurements. However, the detection of covariance between slow and fast oscillations may in itself allow interesting links to be established to the animal literature that would not be possible on the basis of ERPs and ERFs alone.

Acknowledgments

We thank Jens-Max Hopf and Alan Richardson-Klavehn for valuable comments on earlier versions of this manuscript. This study was supported by grants from the Deutsche Forschungsgemeinschaft (DFG/SFB 426, TP C7).

References

Baayen, R.L., Piepenbrock, R., Von Rijn, H. 1993. The CELEX lexical database. CD-ROM. Linguistic Data Consortium, Univ. of Pennsylvania, Philadelphia.

Basar, E., Schurman, M., Basar-Eroglu, C., Demiralp, T., 2001. Selectively distributed gamma band system of the brain. Int. J. Psychophysiology 39, 129–135.

Basar-Eroglu, C., and Demiralp, T., 2001. Event-related theta oscillations: an integrative and comparative approach in the human and animal brain. Int. J. Psychophysiol. 39, 167–195.

Braun, A.R., Balkin, T.J., Wesensten, N.J., Gwadry, F., Carson, R.E., Varga, M., Baldwin, P., Belenky, G., and Herscovitch, P., 1998. Dissociated pattern of activity in visual cortices and their projections during human rapid eye movement sleep. Science 279, 91–95.

Burgess, A.P., Gruzelier, J.H., 2000. Short duration power changes in EEG during recognition memory for words and faces. Psychophysiology 37, 596–606.

Buzsaki, G., 1996. The hippocampo-neocortical dialogue. Cereb. Cortex 6, 81–92.

Buzsaki, G., 2002. Theta oscillations in the hippocampus. Neuron 33, 325–340.

Crouzeix, A., Yvert, B., Bertrand, O., and Pernier, J., 1999. An evaluation of dipole reconstruction accuracy with spherical and realistic head models in MEG. Clin. Neurophysiol. 110, 2176–2188.

Curran, T., 2000. Brain potentials of recollection and familiarity. Memory Cogn. 28, 923–938.

Dale, A.M., Liu, A.K., Fischi, B.R., Buckner, R.L., Belliveau, J.W., Lewine, J.D., Halgren, E., 2000. Dynamic statistical parametric mapping: combining fMRI and MEG for high-resolution imaging of cortical activity. Neuron 26, 55–67.

Duzel, E., Cabeza, R., Picton, T.W., Yonelinas, A.P., Scheich, H., Heinze, H.J., Tulving, E., 1999. Task-related and item-related brain processes of memory retrieval. Proc. Natl. Acad. Sci. USA 96, 1794–1799.

Duzel, E., Picton, T.W., Cabeza, R., Yonelinas, A.P., Scheich, H., Heinze, H.J., Tulving, E., 2001. Comparative electrophysiological and hemodynamic measures of neural activation during memory-retrieval. Hum. Brain Mapp. 13, 104–123.

Duzel, E., Vargha-Khadem, F., Heinze, H.J., Mishkin, M., 2001. Brain activity evidence for recognition without recollection after early hippocampal damage. Proc. Natl. Acad. Sci. USA 98, 8101–8106.

Duzel, E., Yonelinas, A.P., Mangun, G.R., Heinze, H.J., Tulving, E., 1997. Event-related brain potential correlates of two states of conscious awareness in memory. Proc. Natl. Acad. Sci. USA 94, 5973–5978.

Efron, B., Tibshirani, R., 1986. Bootstrap methods for standard errors, confidence intervals and other measures of statistical accuracy. Stat. Sci. STKE 1, 54–77.

Elger, C.E., Grunwald, T., Lehnertz, K., Kutas, M., Helmstaedter, C., Brockhaus, A., Van Roost, D., Heinze, H.J., 1997. Human temporal lobe potentials in verbal learning and memory processes. Neuropsychologia 35, 657–667.

Fabiani, M., Friedman, D., Cheng, J.C., 1998. Individual differences in P3 scalp distribution in older adults, and their relationship to frontal lobe function. Psychophysiology 35, 698–708.

Fernandez, G., Effern, A., Grunwald, T., Pezer, N., Lehnertz, K., Dumpelmann, M., Van Roost, D., Elger, C.E., 1999. Real-time tracking of memory formation in the human rhinal cortex and hippocampus [see comments]. Science 285, 1582–1585.

Fuchs, M., Drenckhahn, R., Wischmann, H.A., Wagner, M., 1998. An improved boundary element method for realistic volume-conductor modeling. Trans. Biomed. Eng. 45, 980–997.

Fuchs, M., Wagner, M., Köhler, T., Wischmann, H.A., 1999. Linear and nonlinear current density reconstructions. J. Clin. Neurophysiol. 16, 267–295.

Fuchs, M., Wagner, M., Wischmann, H.A., Kohler, T., Theissen, A., Drenckhahn, R., Buchner, H., 1998. Improving source reconstructions

by combining bioelectric and biomagnetic data. Electroencephalogr. Clin. Neurophysiol. 107, 93–111.
Galambos, R., Makeig, S., Talmachoff, P.J., 1981. A 40-Hz auditory potential recorded from the human scalp. Proc. Natl. Acad. Sci. USA 78, 2643–2647.
Green, J.D., Arduini, A.A., 1954. Hippocampal electrical activity in arousal. J. Neurophysiol. 17, 533–547.
Grunwald, T., Lehnertz, K., Heinze, H.J., Helmstaedter, C., Elger, C.E., 1998. Verbal novelty detection within the human hippocampus proper. Proc. Natl. Acad. Sci. USA 95, 3193–3197.
Hämäläinen, M.S., Sarvas, J., 1989. Realistic conductivity geometry model of the human head for interpretation of neuromagnetic data. IEEE Trans. Biomed. Eng. 36, 165–171.
Heit, G., Smith, M.E., Halgren, E., 1990. Neuronal activity in the human medial temporal lobe during recognition memory. Brain 113, 1093–1112.
Henson, R.N., Rugg, M.D., Shallice, T., Josephs, O., and Dolan, R.J., 1999. Recollection and familiarity in recognition memory: an event-related functional magnetic resonance imaging study. J. Neurosci. 19, 3962–3972.
Hopf, M., Luck, S.J., Girelli, M., Hagner, T., Mangun, R., Scheich, H., Heinze, H.J. 2001. Neural sources of focused attention in visual search. Cereb. Cortex 10, 1233–1241.
Klimesch, W., Doppelmayr, M., Schwaiger, J., Winkler, T., Gruber, W., 2000. Theta oscillations and the ERP old/new effect: independent phenomena? Clin. Neurophysiol. 111, 781–793.
Klimesch, W., Doppelmayr, M., Yonelinas, A., Kroll, N.E., Lazzara, M., Rohm, D., Gruber, W., 2001. Theta synchronization during episodic retrieval: neural correlates of conscious awareness. Brain Res. Cogn. Brain Res. 12, 33–38.
Klimesch, W., Schimke, H., Doppelmayr, M., Ripper, B., Schwaiger, J., Pfurtscheller, G., 1996. Event-related desynchronization (ERD) and the Dm effect: does alpha desynchronization during encoding predict later recall performance? Int. J. Psychophysiol. 24, 47–60.
Kopell, N., Ermentrout, G.B., Whittington, M.A., Traub, R.D., 2000. Gamma rhythms and beta rhythms have different synchronization properties. Proc. Natl. Acad. Sci. USA 97, 1867–1872.
Lepage, M., Ghaffar, O., Nyberg, L., Tulving, E., 2000. Prefrontal cortex and episodic memory retrieval mode. Proc. Natl. Acad. Sci. USA 97, 506–511.
Lobaugh, N.J., West, R., Mcintosh, A.R., 2001. Spatiotemporal analysis of experimental differences in event-related potential data with partial least squares. Psychophysiology 38, 517–530.
Logothetis, N.K., Pauls, J., Augath, M., Trinath, T., Oeltermann, A., 2001. Neurophysiological investigation of the basis of the fMRI signal. Nature 412, 150–157.
Lopes Da Silva, F., 1991. Neural mechanisms underlying brain waves: from neural membranes to networks. Electroencephalogr. Clin. Neurophysiol. 79, 81–93.
Mcintosh, A.R., Bookstein, F.L., Haxby, J.V., Grady, C.L., 1996. Spatial pattern analysis of functional brain images using partial least squares. NeuroImage 3, 143–157.
Niedermeyer, E., 1997. Alpha rhythms as physiological and abnormal phenomena. Int. J. Psychophysiol. 26, 31–49.
O'keefe, J., Burgess, N., 1999. Theta activity, virtual navigation and the human hippocampus. Trends Cogn. Sci. 3, 403–406.
Paller, K.A., Kutas, M., Mcisaac, H.K., 1995. Monitoring conscious recollection via the electrical activity of the brain. Psychol. Sci. 6, 107–111.
Petsche, H., Stumpf, C., Gogolak, G., 1962. The significance of the rabbit's septum as a relay station between the midbrain and the hippocampus. The control of hippocampus arousal by septum cells. Electroencephalogr. Clin. Neurophysiol. 14, 202–211.
Pfurtscheller, G., Aranibar, A., 1977. Event-related cortical desynchronisation detected by power measurements of scalp EEG. Electroencephalogr. Clin. Neurophysiol. 42, 817–826.
Rolls, E.T., 1996. A theory of hippocampal function in memory. Hippocampus 6, 601–620.
Rugg, M.D., Mark, R.E., Walla, P., Schloerscheidt, A.M., Birch, C.S., Allan, K., 1998. Dissociation of the neural correlates of implicit and explicit memory. Nature 392, 595–598.
Sampson, P.D., Streissguth, A.P., Barr, H.M., Bookstein, F.L., 1989. Neurobehavioral effects of prenatal alchohol: Part II. Partial least squares analysis. Neurotox. Teratol. 11, 477–491.
Schurmann, M., Basar, E., 2001. Functional aspects of alpha oscillations in the EEG. Int. J. Psychophysiol. 39, 151–158.
Smith, M.E., 1987. Electrophysiology of human memory: scalp and intracranial event-related potentials recorded during recognition judgments and related tasks. Diss. Abstr. Int. 47, 4330.
Steriade, M., Gloor, P., Llinas, R.R., Lopes De Silva, F.H., Mesulam, M.M., 1990. Report of IFCN Committee on Basic Mechanisms. Basic mechanisms of cerebral rhythmic activities. Electroencephalogr. Clin. Neurophysiol. 76, 481–508.
Talairach, and Toumoux, 1988. Coplanar Stereotaxic Atlas of the Human Brain. Thieme Medical, New York.
Tallon-Baudry, C., Bertrand, O., 1999. Oscillatory gamma activity in humans and its role in object representation. Trends Cogn. Sci. 3, 151–162.
Tendolkar, I., Rugg, M., Fell, J., Vogt, H., Scholz, M., Hinrichs, H., Heinze, H.J., 2000. A magnetoencephalographic study of brain activity related to recognition memory in healthy young human subjects. Neurosci. Lett. 280, 69–72.
Tesche, C.D., Karhu, J., 2000. Theta oscillations index human hippocampal activation during a working memory task. Proc. Natl. Acad. Sci. USA 97, 919–924.
Vanderwolf, C.H., 1969. Electroencephalogr. Clin. Neurophysiol. 26, 407–418.
Varela, F., Lachaux, J.P., Rodriguez, E., Martinerie, J., 2001. The brainweb: phase synchronization and large-scale integration. Nature Rev. Neurosci 2, 229–239.
Vargha-Khadem, F., Gadian, D.G., Watkins, K.E., Connelly, A., Van Paesschen, W., Mishkin, M., 1997. Differential effects of early hippocampal pathology on episodic and semantic memory. Science 277, 376–380.